



ELSEVIER

Journal of Electron Spectroscopy and Related Phenomena 117–118 (2001) 517–526

JOURNAL OF  
ELECTRON SPECTROSCOPY  
and Related Phenomena

www.elsevier.nl/locate/elspec

## Recent high resolution photoemission studies of electronic structure in quasi-one-dimensional conductors

Kevin E. Smith<sup>a,\*</sup>, Jinyu Xue<sup>a</sup>, Laurent Duda<sup>a</sup>, Alexei Federov<sup>b</sup>, Peter D. Johnson<sup>b</sup>, Steve L. Hulbert<sup>c</sup>, William McCarroll<sup>d</sup>, Martha Greenblatt<sup>d</sup>

<sup>a</sup>Department of Physics, Boston University, 590 Commonwealth Ave., Boston, MA 02215, USA

<sup>b</sup>Department of Physics, Brookhaven National Laboratory, Upton, NY 11973, USA

<sup>c</sup>National Synchrotron Light Source, Brookhaven National Laboratory, Upton, NY 11973, USA

<sup>d</sup>Department of Chemistry, Rutgers University, New Brunswick, NJ 08903, USA

Received 28 August 2000; accepted 19 September 2000

### Abstract

The electronic structure near the Fermi level of  $K_{0.3}MoO_3$  and  $Li_{0.9}Mo_6O_{17}$ , two prototypical quasi-one-dimensional (1D) conductors, has been studied using very high resolution angle-resolved photoemission spectroscopy. Our results differ from earlier lower resolution studies. For  $Li_{0.9}Mo_6O_{17}$  we clearly observe a quasi-1D state dispersing through the Fermi level ( $E_F$ ) and the opening up of a gap at  $E_F$  as the sample is cooled through a bulk metal to non-metal transition at 24 K. For  $K_{0.3}MoO_3$  we clearly observe two quasi-1D bands cross  $E_F$ , and measured a temperature dependence to the Fermi surface nesting vector that correlates well with neutron-scattering measurements of the charge density wave vector. © 2001 Elsevier Science B.V. All rights reserved.

**Keywords:** One-dimensional metals; Photoemission spectroscopy; Charge density waves; Neutron scattering; Fermi surfaces

### 1. Introduction

The interpretation of the results of angle resolved photoemission (ARP) studies of the electronic structure of quasi-one-dimensional (1D) solids is highly controversial [1–4]. ARP should, in principle, provide unique information about quasi-1D solids, including the full structure of the Fermi surface, and about possible non-Fermi liquid behavior of electrons close to the Fermi level ( $E_F$ ). In practice, many aspects of the spectroscopy make straightforward

interpretation of the spectra difficult. Not least of these is its surface sensitivity, which often puts significant limitations on its application [4]. It has been reported that photoemission from states near  $E_F$  in quasi-1D conductors differs significantly from that measured from two- and three-dimensional solids, with (among other differences) an anomalously low emission intensity at  $E_F$  [1,2,5–10]. There are a number of possible explanations for these observations, including problems with surface defects and stoichiometry [4,11,12], charge density wave (CDW) fluctuations leading to a pseudogap [13], or a Luttinger liquid state [14–19].

We have performed temperature dependent ARP studies of the electronic structure close to  $E_F$  in the

\*Corresponding author. Tel.: +1-617-353-6117; fax: +1-617-353-9393.

E-mail address: ksmith@bu.edu (K.E. Smith).

quasi-1D conductors  $\text{Li}_{0.9}\text{Mo}_6\text{O}_{17}$  and  $\text{K}_{0.3}\text{MoO}_3$  [20,21]. These materials are members of a class of quasi-low dimensional conductors known as molybdenum oxide bronzes. Molybdenum bronzes are ideal for ARP studies since large high quality crystals can be grown [22,23], and surfaces suitable for ARP measurements can be prepared by cleaving the crystals in vacuum [4].

$\text{Li}_{0.9}\text{Mo}_6\text{O}_{17}$  is metallic at room temperature, becomes semiconducting at 24 K, and finally becomes superconducting at 1.9 K [22,24]. It is unknown whether the transition at 24 K is caused by a CDW or a spin density wave (SDW). A tight binding band structure calculation for  $\text{Li}_{0.9}\text{Mo}_6\text{O}_{17}$  predicts two fully occupied and two partially occupied Mo 4d-derived bands within 0.3 eV of  $E_F$  for states along the quasi-1D conducting direction [25]. The two partially filled bands are degenerate at  $E_F$ , and the predicted Fermi surface for  $\text{Li}_{0.9}\text{Mo}_6\text{O}_{17}$  consists of two parallel straight lines.

$\text{K}_{0.3}\text{MoO}_3$  is also metallic at room temperature, and undergoes a Peierls transition at 180 K to a CDW state. Tight binding band structure calculations for  $\text{K}_{0.3}\text{MoO}_3$  predict two partially occupied Mo 4d-derived bands crossing  $E_F$  along the quasi-1D conducting direction, forming two discrete nested Fermi surface sheets [26]. Diffraction studies reveal a single CDW with wave vector along the quasi-1D  $b$ -direction [27–29]. It was also found that, along this direction, the CDW wave vector ( $q_{\text{CDW}}$ ) is temperature-dependent. At higher temperatures it is incommensurate and at  $\sim 100$  K it approaches the value expected in a commensurate phase, i.e.  $\sim 0.75b^*$  ( $b^* = 2\pi/b$  is the reciprocal lattice unit corresponding to the quasi-1D direction). This value relates directly to the Fermi surface nesting given by band structure calculations that predict two Fermi wave vectors,  $k_{F1} = 0.33b^* = 0.274 \text{ \AA}^{-1}$  and  $k_{F2} = 0.42b^* = 0.349 \text{ \AA}^{-1}$ , yielding a nesting vector ( $k_{F1} + k_{F2}$ ) =  $0.75b^* = 0.623 \text{ \AA}^{-1}$ .

## 2. Experimental method

Our experiments were carried out on undulator beam line U13UB at the National Synchrotron Light Source, Brookhaven National Laboratory. The ARP

measurements were performed using a commercial SES 200 Scienta hemispherical analyzer, modified so that the total spectral response can be measured as a function of angle and energy simultaneously. Operated in such a mode, the angular resolution of the analyzer is approximately  $\pm 0.1^\circ$  and the total energy resolution reached in the present measurements was approximately 15 meV (for the  $\text{K}_{0.3}\text{MoO}_3$  experiments) or 33 meV (for the  $\text{Li}_{0.9}\text{Mo}_6\text{O}_{17}$  experiments) at temperatures between 17 and 300 K, and at a photon energy of 21.4 eV. The Fermi energy and the energy resolution were determined by evaporating either a gold or a gadolinium film onto the sample and measuring the Fermi distribution cut-off. For the photon energy employed here, the instrument angular resolution results in a momentum resolution of better than  $0.01 \text{ \AA}^{-1}$ , which is crucial for resolving a rapidly dispersing band. The  $\text{K}_{0.3}\text{MoO}_3$  and  $\text{Li}_{0.9}\text{Mo}_6\text{O}_{17}$  single crystals were grown by a temperature gradient flux technique reported elsewhere [24,30]. Clean surfaces were obtained by cleaving the sample in situ in the measurement chamber, which had a base pressure of  $2 \times 10^{-11}$  Torr. In order to avoid electron damage to the surface [4,11,12], each sample was cleaved twice before taking spectra. After the first cleave, low energy electron diffraction (LEED) was used to determine the orientation of the crystal with respect to the polarization vector of the radiation and the spectrometer axis. The sample was then cleaved again in the desired orientation to expose a new surface for photoemission measurements. Cooling of the samples was achieved using a liquid He cryostat. Sample temperature was monitored using a silicon diode attached to the sample holder. At the completion of the experiment the diode was then calibrated against another directly attached to the sample in order to account for the temperature gradient between the holder and the sample.

## 3. Results

### 3.1. $\text{Li}_{0.9}\text{Mo}_6\text{O}_{17}$

Fig. 1 presents the photoemission intensity map of the total spectral response for photoemission from  $\text{Li}_{0.9}\text{Mo}_6\text{O}_{17}$  measured at room temperature [20].

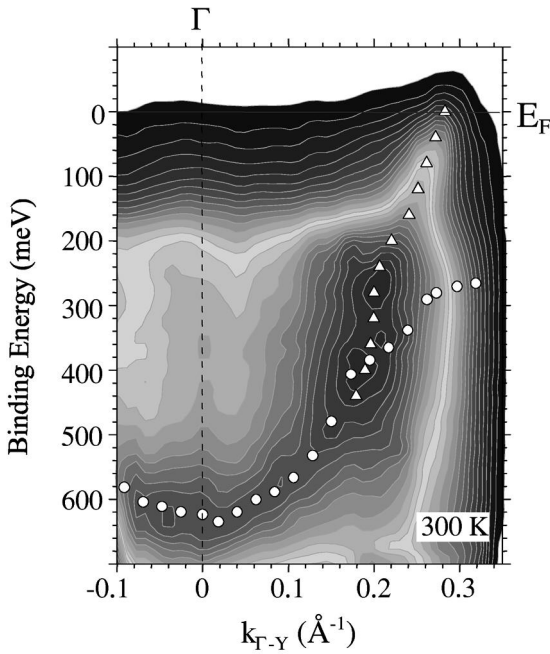


Fig. 1. Intensity map of photoemission from  $\text{Li}_{0.9}\text{Mo}_6\text{O}_{17}$ .  $T=300$  K,  $h\nu=21.4$  eV. Also plotted is the experimentally determined dispersion of d-bands; open triangles are transitions determined from MDCs and the open circles those determined from EDCs. See text for details.

The horizontal axis is angle of emission, converted to the equivalent  $k$ -space values [31]. Two dispersive features are observed within 700 meV of  $E_F$ . One feature disperses symmetrically around the Brillouin zone center ( $\Gamma$  point) and reaches a maximum binding energy of approximately 630 meV at  $\Gamma$ . A second feature splits from the first band, and disperses across  $E_F$ . The dispersion of the bands is indicated in Fig. 1 as filled and open symbols overlaid on the intensity map. The values of these points are extracted from both energy distribution curves (EDCs) and momentum distribution curves (MDCs). By slicing the intensity map of Fig. 1 at a constant value of the emission angle, conventional photoemission spectra are generated; i.e. plots of photoemission intensity versus energy, or EDCs. By slicing the intensity map of Fig. 1 at a constant value of the binding energy, plots of photoemission intensity versus angle (and hence momentum) are generated, and called MDCs. Dispersion determined from EDCs is usually not as accurate as that from

MDCs for a rapidly dispersing band. We therefore used the MDCs to identify the location of the band crossing  $E_F$ . Data taken at 27 K (not shown) also display only one emission feature crossing  $E_F$ .

Fig. 2 shows the EDCs close to  $k_F$  for states along the quasi-1D direction ( $\Gamma Y$ ), extracted from the data of Fig. 1. The dispersion of a state across  $E_F$  is clearly visible. The data in Figs. 1 and 2 reveal considerable photoemission intensity at  $E_F$  as the band crosses the Fermi surface. The well-defined crossing enables the determination of the nesting vector of the Fermi surface. With  $k_F=0.28 \text{ \AA}^{-1}$ , the nesting wave vector is therefore  $2k_F=0.56 \text{ \AA}^{-1}$ . We

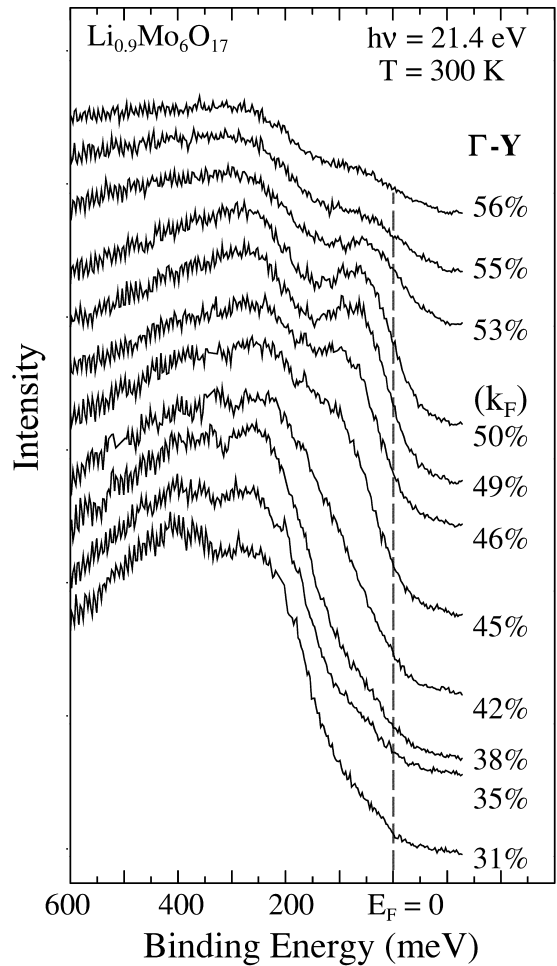


Fig. 2. EDCs extracted from the intensity map (Fig. 1) for states along the  $\Gamma Y$  direction at room temperature.  $T=300$  K,  $h\nu=21.4$  eV.

also determined  $2k_F$  by directly measuring the distance in reciprocal space of two symmetric bands crossing the Fermi surface in the first Brillouin zone and obtained the same value.

In Fig. 3 we show EDCs corresponding to  $k = k_F$ , taken with the sample at 300 and 17 K, above and below the metal-semiconductor transition temperature. The spectral function in our experiment exhibits significant intensity at  $E_F$  for the sample at room temperature and this intensity is non-zero even at 17 K when resistivity measurements indicate that a gap has opened [24]. The leading edge shift of the spectra between 300 and 17 K is estimated to be approximately 40 meV giving a total gap opening of 2–80 meV. Fig. 4 presents the  $k$ -integrated emission spectrum at room temperature, for  $k$  close to  $k_F$ . This spectrum is obtained by integrating the data of Fig. 1 around  $k_F$  over an angular window of  $2^\circ$  (approximately  $0.2 \text{ \AA}^{-1}$ ). This is large enough to reflect the

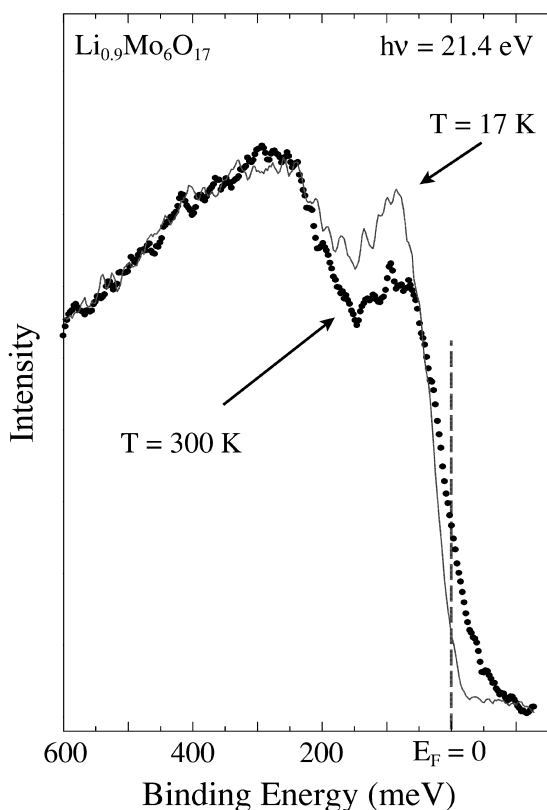


Fig. 3. EDCs extracted from the intensity map (Fig. 1) for states at  $k_F$  with the sample at 300 and 17 K.  $h\nu = 21.4 \text{ eV}$ .

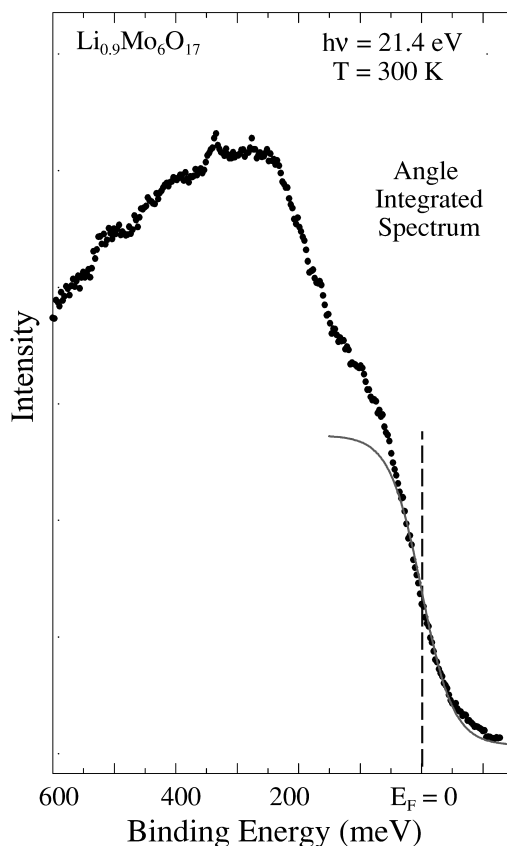


Fig. 4. Angle integrated spectrum (open circles) and the Fermi function (solid line), both at 300 K. The spectrum is obtained by integrating the intensity map for states around  $k = k_F$ . See text for details.

density of states (DOS) for the band crossing the Fermi surface since the band disperses rapidly. With an energy resolution of 33 meV in this experiment, the resolution broadening is negligible compared with the large thermal broadening at 300 K. Fig. 4 also shows that the spectral intensity near  $E_F$  matches the Fermi function at 300 K. This is in contrast to the vanishing spectral weight at  $E_F$ , as measured by angle-integrated photoemission for many quasi-1D metals [4].

### 3.2. $K_{0.3}MoO_3$

Fig. 5a presents the photoemission intensity map of the total spectral response for photoemission from

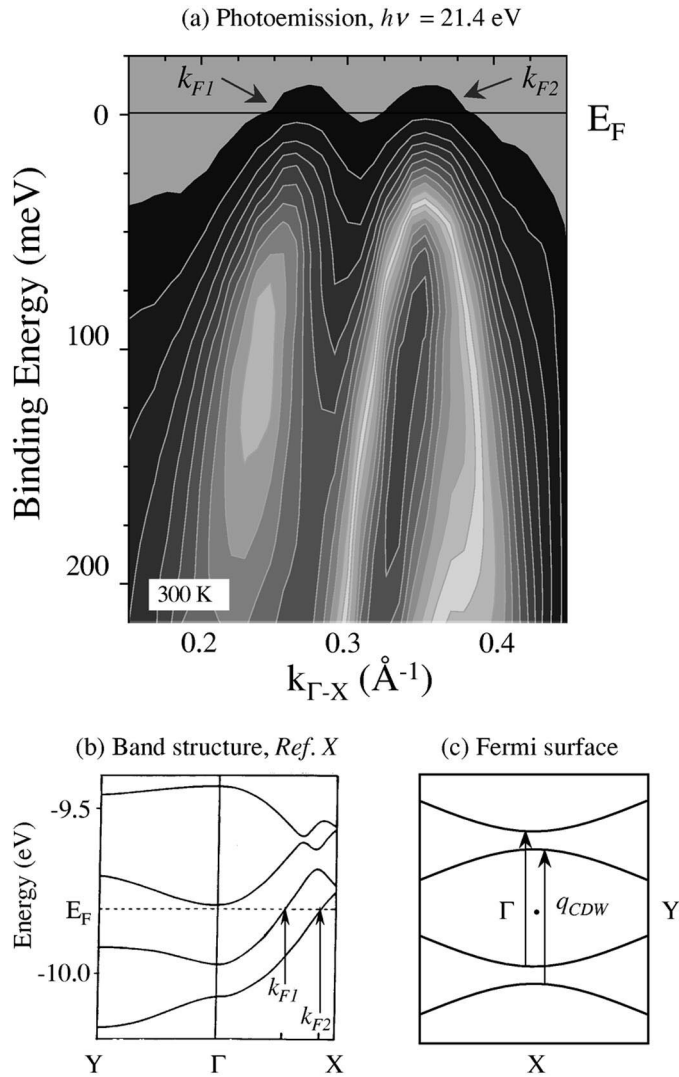


Fig. 5. (a) Photoemission intensity map of  $\text{K}_{0.3}\text{MoO}_3$ ; (b) calculated band structure of  $\text{K}_{0.3}\text{MoO}_3$  from Ref. [26]. (c) Schematic of the Fermi surface.

$\text{K}_{0.3}\text{MoO}_3$  in the region close to the Fermi level crossings, measured at room temperature [21]. The experimental data reveal the existence of two bands that are parallel in the vicinity of the Fermi level and split by  $\sim 480$  meV. Fig. 5b shows the results of a tight binding band structure calculation and the experimentally observed emission features in Fig. 5a are clearly related to the bands found in the calculation, indicating that they are formed by the d-bands of Mo [26]. The calculated splitting of 160 meV is,

however, three times smaller than that found experimentally. In Fig. 5c, we show a schematic Fermi surface. It is composed of two lines of opposite curvature, suggesting that the lower Fermi surface of the first band is nested to the upper Fermi surface of the second band and vice versa [26,28]. Consequently, the single CDW observed in X-ray and neutron scattering experiments has a wave vector which equals the sum of the two Fermi wave vectors,  $(k_{F1} + k_{F2})$ . These wave vectors can now be de-

terminated with high precision using the data of Fig. 5a.

In general, there are two ways of using ARP to measure Fermi wavevectors. The first involves measuring a series of EDCs, and tracking the dispersion of an emission feature as it crosses above  $E_F$ . This is quite sufficient in simple systems, but becomes problematic in complex conductors since knowledge of model spectral functions is required, which is an area of intense theoretical discussion [32–34]. Alternatively, one can measure the intensity of photoelectrons versus momentum at  $E_F$ . Such a

method was in fact successfully used for measuring the Fermi surface in the normal state of the high temperature superconductor  $\text{Bi}_2\text{Sr}_2\text{CaCu}_2\text{O}_8$ , which is characterized by the absence of well-defined quasiparticle excitations [35]. Exploiting the natural capabilities of our spectrometer, we use the latter method. The procedure simply consists of taking intensity versus momentum profiles at  $E_F$  from the ARP map in Fig. 5a and identifying the points of highest intensity.

Fig. 6 shows the photoemission intensity at  $E_F$  as a function of sample temperature and momentum.

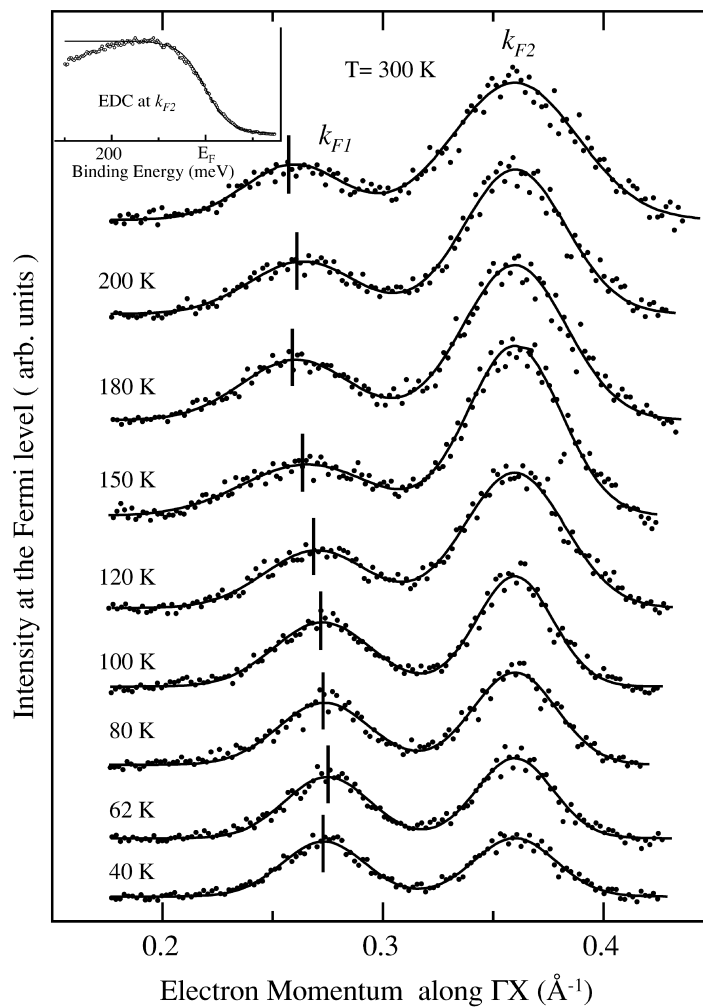


Fig. 6. Results of the least-square fit analysis of intensity versus electron momentum profiles at the Fermi level. The inset shows the EDC measured at the emission angle corresponding to the Fermi wave vector  $k_{F2}$ . The solid line represents experimentally determined Fermi edge measured from an evaporated gold film.

This set of constant energy profiles was obtained by integrating the temperature dependent 3D ARP maps in an energy window of  $E_F \approx 5$  meV. Each profile consists of two well-defined peaks, corresponding to the two bands crossing  $E_F$ , from which  $k_{F1}$  and  $k_{F2}$  can be immediately identified. To verify that they do correspond to Fermi level crossings, we produced traditional EDCs by cutting the photocurrent map in an angular window of  $0.2^\circ$  centered at angle corresponding to  $k_{F2}$ . The result is shown as an inset in Fig. 6. The solid line through the data points is a Fermi edge of the Au film deposited on the sample. We clearly observe significant intensity at  $E_F$ , and an unambiguous Fermi cut-off. This is in sharp contrast to earlier reports based on the use of an electron spectrometer with conventional, i.e.  $\approx 1^\circ$ , angular resolution [6]. (Significantly, we found that cutting the intensity map at slightly different angles or using a window of  $2^\circ$  results in EDCs with intensity greatly suppressed at  $E_F$ ) When the temperature is lowered below 180 K, the intensity of both peaks gradually decreases, reflecting the gap opening at  $E_F$  associated with the Peierls transition. The data reveal that the gap does not open fully, and there is enough intensity at  $E_F$  for us to track the position of the Fermi wave vector(s) through the Peierls transition. This could either be due to fluctuations of the CDW order parameter [36], or the formation of amplitude solitons [37]. However, the data of Fig. 6 also show that there is a reduction of the splitting between the peaks, implying an increase of  $(k_{F1} + k_{F2})$  for temperatures between 180 and 100 K. This increase is dominated by the movement of  $k_{F1}$  towards  $k_{F2}$ . While the former exhibits strong temperature dependence, the latter does not appear to show any systematic shift with temperature, but we cannot exclude a slight temperature dependence of  $k_{F2}$  beyond our momentum resolution.

For a more quantitative analysis, the constant energy profiles were fit using a least-squares procedure to two Gaussians representing peaks at  $k_{F1}$  and  $k_{F2}$ , respectively. A linear background was superimposed to account for scattered electrons. The intrinsic widths of the Gaussians were found to decrease slightly upon cooling the sample. The solid line through the data points in Fig. 6 represents the results of the fit. The value of  $\{1 - (k_{F1} + k_{F2})\}$  determined in this manner is plotted versus tempera-

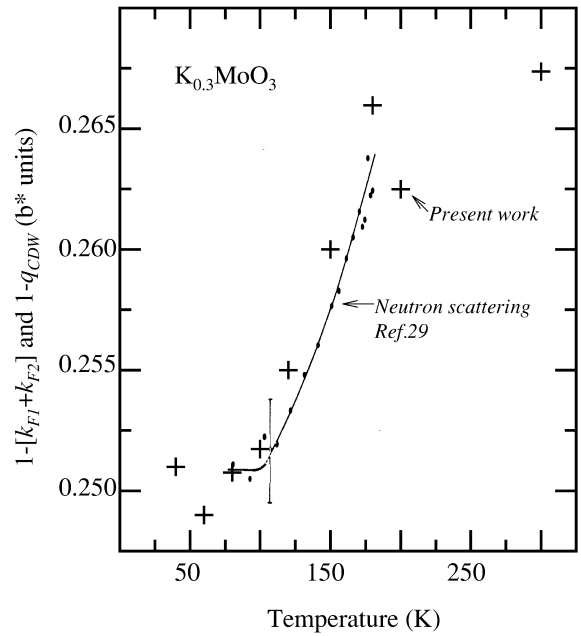


Fig. 7. Temperature dependence of  $[1 - (k_{F1} + k_{F2})]$  derived from the data in Fig. 6 (crosses) and temperature dependence of  $(1 - q_{CDW})$  measured by neutron-scattering.

ture in Fig. 7. On the same figure, we have also shown the temperature dependence of the reduced wave vector of the CDW,  $(1 - q_{CDW})$ , obtained from inelastic neutron scattering [29]. The two curves coincide well, showing that the temperature dependence of the nesting wave vector is due to that of the Fermi wave vector.

## 4. Discussion

### 4.1. $Li_{0.9}Mo_6O_{17}$

In an earlier lower resolution ARP study of  $Li_{0.9}Mo_6O_{17}$  we measured the Fermi surface by mapping a discontinuity in the dispersion of the d-band emission near  $E_F$  [38]. This study verified the shape of the Fermi surface, but the measured nesting vector was larger ( $0.7 \text{ \AA}^{-1}$ ) than expected from the calculations, and we did not observe much of the predicted band dispersion [25]. Subsequently, Gweon et al. [6] also studied  $Li_{0.9}Mo_6O_{17}$  using ARP. Their

experiment was performed with better energy resolution and with the sample at a lower temperature than our earlier study, but they also were unable to fully resolve the predicted band dispersion. Both studies revealed little spectral weight at  $E_F$ . The most recent ARP study of  $\text{Li}_{0.9}\text{Mo}_6\text{O}_{17}$  by Denlinger et al. [39], performed with an energy resolution of 50 meV and an angular resolution of  $\approx 1^\circ$ , did observe some band dispersion, but again could not observe any emission intensity at  $E_F$ .

Clearly, Fig. 1 shows a dispersive state crossing  $E_F$ . We attribute our observation of the dispersive state to our very high energy and momentum resolution, as well as a careful alignment by LEED of the orientation of the sample; even a small misalignment of the sample orientation leads to significant changes in the spectra. We have not resolved all the predicted bands, but have clearly observed the predicted band splitting near  $k_F$  [25]. As noted above, the well-defined crossing enables the determination of the nesting vector of the Fermi surface to be  $2k_F = 0.56 \text{ \AA}^{-1}$ . This value is slightly larger than predicted by theory ( $2k_F = 0.51 \text{ \AA}^{-1}$ ) [25], but closer than that obtained in our previous lower resolution measurement [38]. It is essentially the same as that reported by Denlinger et al. [39]. The total measured dispersion of the d-band below  $E_F$  is larger by a factor of 2 than predicted [25]. Such a discrepancy has also been observed in earlier measurements for  $\text{K}_{0.3}\text{MoO}_3$  and  $\text{Li}_{0.9}\text{Mo}_6\text{O}_{17}$  [6].

The observation of the Fermi cut-off in Fig. 4 can be understood as evidence for 3D metallic behavior. Despite the quasi-1D transport and optical properties of  $\text{Li}_{0.9}\text{Mo}_6\text{O}_{17}$ , it has a pronounced 3D crystal structure [22,24], and a large Debye temperature [22]. Furthermore, a significant interaction between the  $\text{Mo}_4\text{O}_{18}$  chains parallel to the  $b$ -axis is predicted [25]. This interchain coupling was evident in our earlier observation of slight dispersion of the d-band perpendicular to the 1D chain of  $\text{Li}_{0.9}\text{Mo}_6\text{O}_{17}$  [38]. The interchain coupling reduces the 1D metallic character and may give rise to 3D electron dynamics, resulting in a Fermi liquid. In a pure 1D interacting electron system, the low energy excitations are correctly described by a Luttinger liquid, and electron–electron interactions are predicted to induce a strong suppression of the photoemission intensity at  $E_F$  [2,14]. Furthermore, the  $\mathbf{k}$ -integrated single-par-

ticle spectrum of a Luttinger liquid exhibits a power-law dependence of the electron binding energy near  $E_F$ , and the lineshape of the spectral function ( $k$ -resolved single-particle spectrum) depends strongly on the value of the correlation exponent  $a$  [2,19,40,41]. If we attempt to interpret our spectra in a Luttinger framework, then given that we clearly observe a Fermi surface crossing,  $\text{Li}_{0.9}\text{Mo}_6\text{O}_{17}$  must fall in the small- $a$  class ( $a \leq 1$ ) of the Luttinger electron system [2]. However, no separate peaks are observed in our measured EDCs or MDCs that can be interpreted as due to holons and spinons, and this puts a lower limit of 0.5 on  $a$  [2,19,40,41]. At best, if our data is interpreted in a Luttinger framework, then  $\text{Li}_{0.9}\text{Mo}_6\text{O}_{17}$  has  $0.5 \leq a \leq 1$ .

#### 4.2. $\text{K}_{0.3}\text{MoO}_3$

As noted above,  $q_{\text{CDW}}$  is temperature dependent in  $\text{K}_{0.3}\text{MoO}_3$ . In order to explain this, Pouget et al. [28] suggested that there exists a flat band just above  $E_F$  in  $\text{K}_{0.3}\text{MoO}_3$  which can be thermally populated. The temperature dependence of  $q_{\text{CDW}}$  can then be attributed to charge transfer between the two bands crossing  $E_F$  and the third band. This would also account for the temperature dependence of  $k_F$ . While band structure calculations do indeed show a third band located at 0.012 eV above  $E_F$  at  $\Gamma$ , this band disperses rapidly to higher energies away from the zone center [26]. If this band were thermally populated, then there would be a continuous change in  $k_F$  between 180 K and 300 K. However, our results indicate that the variation in  $k_F$  is much smaller at higher temperatures, thereby ruling out a simple charge transfer model. An explanation for the temperature dependence of the nesting wave has been proposed by Noguera and Pouget [42], who showed that a nonlinear electron dispersion as well as a finite phonon dispersion can lead to the thermal dependence of the nesting wave vector. Artemenko et al. [43] also proposed a similar explanation. In both models, the thermal dependence of the nesting wave vector follows from a shift in the chemical potential. However, such models cannot explain our results for the temperature dependence of the Fermi wave vectors obtained at a constant energy  $E_F$ . The absence of any detectable shift of the bands at high binding energies is also not consistent with a shift in

the chemical potential. Indeed, the ARP data show that the temperature dependence of the nesting wave vector in  $\text{K}_{0.3}\text{MoO}_3$  is predominantly (if not completely) due to a change in the electronic structure. Since the change in the Fermi wave vectors of  $\text{K}_{0.3}\text{MoO}_3$  occurs between 100 and 200 K, it is reasonable to associate any change in the electronic structure with a change in the coupling between chains belonging to different unit cells (the smallest electronic scale in the problem). This can happen if for instance, the Mo–O distances in the basal plane change continuously with temperature. To explore this possibility, we have calculated the Fermi surface using a tight binding model, and found a consistent behavior [20].

## 5. Conclusions

In conclusion, we have used high energy and momentum resolution ARP to study the electronic structure close to  $E_F$  in  $\text{Li}_{0.9}\text{Mo}_6\text{O}_{17}$  and  $\text{K}_{0.3}\text{MoO}_3$ . For  $\text{Li}_{0.9}\text{Mo}_6\text{O}_{17}$  we have resolved a band dispersing across  $E_F$ , and found a nesting vector close to that predicted, although the total band width is at least twice as large as predicted [25]. Consistent with resistivity measurements, a gap has been observed to open up in the band structure at  $E_F$  associated with the metal-semiconductor transition. Our observations of Fermi surface crossings and a Fermi function-like density of states are consistent with the room temperature metallic character of this material in the quasi-1D direction. Our observations are not consistent with a recent report of non-Fermi liquid phenomena in  $\text{Li}_{0.9}\text{Mo}_6\text{O}_{17}$  which was based on a line shape analysis of emission spectra from states near  $E_F$  [39]. Using lower energy and momentum resolution than that available in the present study, Denlinger et al. [39] were unable to observe the state forming the Fermi surface, the opening of the gap, nor significant intensity at  $E_F$ . Our data calls into doubt the conclusion of Denlinger et al. [39] that the low energy excitations of electrons in  $\text{Li}_{0.9}\text{Mo}_6\text{O}_{17}$  should be described in a Luttinger liquid model. For  $\text{K}_{0.3}\text{MoO}_3$  we have directly measured two Fermi wave vectors. By monitoring the temperature dependence of the Fermi wave vectors from 300 to 40 K, it was possible for the first time to compare the

temperature dependence of the Fermi wave vectors and the CDW nesting vector. Our results show unambiguously that the temperature dependence of the CDW nesting vector observed in X-ray and neutron scattering experiments is primarily due to a change in the electronic structure.

## Acknowledgements

The Boston University research was supported in part by the US Department of Energy under DE-FG02-98ER45680. The BNL research was supported in part by the US DOE under DE-AC02-98CH10886. Experiments were undertaken at the NSLS, which is supported by the US DOE, Divisions of Materials and Chemical Sciences.

## References

- [1] J.W. Allen, G.H. Gweon, R. Claessen, K. Matho, J. Phys. Chem. Solids 56 (1995) 1849.
- [2] M. Grioni, J. Voit, High resolution photoemission studies of low-dimensional systems, in: H. Stanberg, H. Hughes (Eds.), Electron Spectroscopies Applied to Low Dimensional Materials, Vol. X, 1999, in press.
- [3] M. Grioni, D. Malterre, Y. Baer, J. Low. Temp. Phys. 99 (1995) 195.
- [4] K.E. Smith, Ann. Rep. Prog. Chem. C 90 (1995) 115.
- [5] B. Dardel, D. Malterre, M. Grioni, P. Weibel, Y. Baer, J. Voit, D. Jerome, Europhys. Lett. 24 (1993) 687.
- [6] G.H. Gweon, J.W. Allen, R. Claessen, J.A. Clack, D.M. Poirier, P.J. Benning, C.G. Olson, W.P. Ellis, Y.X. Zhang, L.F. Schneemeyer, J. Marcus, C. Schlenker, J. Phys. Condens. Matter 8 (1996) 9923.
- [7] F. Zwick, D. Jerome, G. Margaritondo, M. Onellion, J. Voit, M. Grioni, Phys. Rev. Lett. 81 (1998) 2974.
- [8] F. Zwick, S. Brown, G. Margaritondo, C. Merlic, M. Onellion, J. Voit, M. Grioni, Phys. Rev. Lett. 79 (1997) 3982.
- [9] F. Zwick, M. Grioni, M. Onellion, L.K. Montgomery, G. Margaritondo, Physica B 265 (1999) 160.
- [10] M. Grioni, I. Vobornik, F. Zwick, G. Margaritondo, J. Electron Spectrosc. Relat. Phenom. 100 (1999) 313.
- [11] K. Breuer, K.E. Smith, M. Greenblatt, W. McCarroll, J. Vac. Sci. Technol. A 12 (1994) 2196.
- [12] K. Breuer, K.E. Smith, M. Greenblatt, W. McCarroll, S.L. Hulbert, J. Phys. Chem. Solids 57 (1996) 1803.
- [13] H.P. Geserich, G. Scheiber, Physica B 143 (1986) 198.
- [14] H.J. Schulz, Physica C 235 (1994) 217.
- [15] J.M. Luttinger, J. Math. Phys. 4 (1963) 1154.
- [16] S. Tomonaga, Prog. Theor. Phys. 5 (1950) 349.
- [17] J. Solyom, Adv. Phys. 28 (1979) 201.

- [18] J. Voit, *Physica C* 282 (1997) 1747.
- [19] J. Voit, *Synth. Met.* 70 (1995) 1015.
- [20] J. Xue, L.-C. Duda, K.E. Smith, A.V. Fedorov, P.D. Johnson, S.L. Hulbert, W.H. McCarroll, M. Greenblatt, *Phys. Rev. Lett.* 83 (1999) 1235.
- [21] A.V. Fedorov, S.A. Brazovskii, V.N. Muthukumar, P.D. Johnson, J. Xue, L.C. Duda, K.E. Smith, W.H. McCarroll, M. Greenblatt, S.L. Hulbert, *J. Phys. Condens. Matter* 12 (2000) L191.
- [22] M. Greenblatt, *Chem. Rev.* 88 (1988) 31.
- [23] C. Schlenker (Ed.), *Low Dimensional Electronic Properties of Molybdenum Bronzes and Oxides*, Kluwer, Dordrecht, 1989.
- [24] M. Greenblatt, W.H. McCarroll, R. Niefeld, M. Croft, J.V. Waszczak, *Solid State Commun.* 51 (1984) 671.
- [25] M.-H. Whangbo, E. Canadell, *J. Am. Chem. Soc.* 110 (1988) 358.
- [26] M.-H. Whangbo, L.F. Schneemeyer, *Inorg. Chem.* 25 (1986) 2424.
- [27] M. Sato, H. Fujishita, S. Hoshino, *J. Phys. C* 16 (1983) L877.
- [28] J.P. Pouget, C. Noguera, A.H. Moudden, R. Moret, *J. Phys.* 46 (1985) 1731.
- [29] R.M. Flemming, L.F. Schneemeyer, D.E. Moncton, *Phys. Rev. B* 31 (1985) 899.
- [30] K.V. Ramanujachary, M. Greenblatt, W.H. McCarroll, *J. Cryst. Growth* 70 (1984) 476.
- [31] S.D. Kevan (Ed.), *Angle Resolved Photoemission*, Elsevier, Amsterdam, 1991.
- [32] Y. Ren, P.W. Anderson, *Phys. Rev. B* 48 (1993) 16662.
- [33] V. Meden, K. Schonhammer, *Phys. Rev. B* 46 (1992) 15753.
- [34] J. Voit, *J. Phys. Condens. Matter* 5 (1993) 8305.
- [35] P. Aebi, J. Osterwalder, P. Schwaller, L. Schlapbach, M. Shimoda, T. Mochiku, K. Kadowaki, *Phys. Rev. Lett.* 72 (1994) 2757.
- [36] G. Grüner, *Density Waves in Solids*, *Frontiers in Physics*, Vol. 89, Addison-Wesley, Reading, 1994.
- [37] S.A. Brazovskii, *Sov. Phys.-JETP* 51 (1980) 342.
- [38] K.E. Smith, K. Breuer, M. Greenblatt, W. McCarroll, *Phys. Rev. Lett.* 70 (1993) 3772.
- [39] J.D. Denlinger, G.-H. Gweon, J.W. Allen, C.G. Olson, J. Marcus, C. Schlenker, L.-S. Hsu, *Phys. Rev. Lett.* 82 (1999) 2540.
- [40] V. Meden, K. Schonhammer, *Phys. Rev. B* 46 (1993) 15753.
- [41] J. Voit, *Rep. Prog. Phys.* 58 (1995) 977.
- [42] C. Noguera, J.P. Pouget, *J. Phys. I* 1 (1991) 1035.
- [43] S.N. Artemenko, *J. Exp. Theor. Phys.* 84 (1997) 823.